

## Article

# Symmetrically Construction Monitoring Analysis and Completed State Evaluation of a Tied Steel Box Arch Bridge Based on Finite Element Method

Jian Pan <sup>1</sup>, Xirui Wang <sup>2,\*</sup> , Kainan Huang <sup>2</sup> and Wensheng Wang <sup>3,\*</sup> <sup>1</sup> Pinglu Canal Group Co., Ltd., Nanning 530000, China; panj\_23@163.com<sup>2</sup> Guangxi Transportation Science and Technology Group Co., Ltd., Nanning 530007, China; 201620105179@mail.scut.edu.cn<sup>3</sup> College of Transportation, Jilin University, Changchun 130025, China

\* Correspondence: wangxr17@mails.jlu.edu.cn (X.W.); wangws@jlu.edu.cn (W.W.)

**Abstract:** Because of their beautiful appearance, strong crossing ability, and reasonable stress performance, the application of tied steel box arch bridges is becoming more and more extensive. Bridge construction monitoring can control and adjust the deviation state to ensure the stress and linear state of the bridge after completion. This study carried out a symmetrical construction monitoring analysis and completed state evaluation of the newly built Dafeng River Bridge in Guangxi Province based on the finite element method. MIDAS Civil finite element software is used for simulation analysis to calculate the deformation and stress of the tied steel box arch bridge at the construction and completion stages. The tensile and compressive stress of the main arch and transverse brace, as well as the cumulative displacements of the main arch and lattice beam, are symmetrically distributed. The maximum tensile and compressive stresses are 15.1 MPa and 74.6 MPa, respectively, less than the specification's allowable value. Meanwhile, for the completed bridge under the loading combinations of serviceability limit state and bearing capacity ultimate limit state, the stress of the main arch, transverse brace, and lattice beam meets the specification requirements. The maximum cable forces of the suspender and tie rod under the bearing capacity ultimate limit state are 2189.4 kN and 2991.2 kN, and their corresponding minimum safety factors are 3.2 and 2.7. In addition, the deviations between the on-site monitoring and the finite element theoretical values are within the specification allowable range for the cable force of the suspender and tie rod and the bridge deck alignment. It indicates that the bridge construction monitoring effect is reasonable and ideal, and the symmetrically finite element simulation analysis can provide a theoretical basis for construction monitoring.

**Keywords:** steel box arch bridge; construction process; bridge monitoring; finite element analysis; structural checking calculation



**Citation:** Pan, J.; Wang, X.; Huang, K.; Wang, W. Symmetrically Construction Monitoring Analysis and Completed State Evaluation of a Tied Steel Box Arch Bridge Based on Finite Element Method. *Symmetry* **2023**, *15*, 932. <https://doi.org/10.3390/sym15040932>

Academic Editor: Zine El Abidine Fellah

Received: 9 March 2023

Revised: 10 April 2023

Accepted: 14 April 2023

Published: 18 April 2023



**Copyright:** © 2023 by the authors. Licensee MDPI, Basel, Switzerland. This article is an open access article distributed under the terms and conditions of the Creative Commons Attribution (CC BY) license (<https://creativecommons.org/licenses/by/4.0/>).

## 1. Introduction

Arch bridges have been widely used in modern transportation and are one of the main forms of long-span bridges due to their beautiful appearance, strong crossing ability, reasonable stress performance, and many other characteristics [1–3]. In view of the continuous development of highway and bridge construction in China, the number of bridges built has increased rapidly [4–6]. With the technological progress of construction level and the improvement in steel, concrete, and other materials, the application of tied steel box arch bridges on roads and bridges is becoming more and more extensive [7–9].

Scholars have made a series of studies on construction monitoring from the aspects of integrity, alignment, cable force, and other characteristics of tied arch bridges [10–12]. The analysis method of space stability of concrete-filled steel tube arch bridge is summarized [13]. Xie et al. [13] summarized the basic theory of structural stability and concrete pouring technology of the largest concrete-filled steel tube arch bridge in the world, the

Guangxi Pingnan Third Bridge, and its linearity, stress, and stability were studied based on construction monitoring. Based on the finite element theory, taking into account the non-linear conditions of structure and material, the construction stability of a tied arch bridge during arch rib concrete pouring was studied by using the ANSYS finite element analysis software [14,15]. The main beam alignment control is a continuous system engineering, and the control results of each stage will have an important impact on the subsequent stages. In the process of bridge construction, experts have begun to consciously pay attention to whether the actual girder alignment of the bridge is consistent with the design alignment, so as to guide the error adjustment [16–18]. Zhang et al. [10] used the long-gauge fiber Bragg grating sensing technology to effectively identify the static and dynamic deflection of the main arch through the derivation of the relationship between strain and deformation on the main arch element, so as to evaluate the structural alignment during construction. Puri et al. [19] used the point cloud data obtained by the mobile laser radar technology and the 4D design model to accurately and effectively monitor each bridge component, so as to track the progress of bridge construction. Cheng et al. [20] used visual observation and total station to monitor the assembly alignment of bridge components, and proposed a pose measurement technology based on stereo vision to continuously track the construction of prefabricated bridge components. There are also many research results at home and abroad on the rational cable force state of the completed bridge during bridge construction [21–23]. Ren et al. [24,25] have studied and established a practical calculation formula for calculating the cable force value. The main calculation parameter is the fundamental frequency of the suspender of the tied arch bridge. Using the ability method and curve fitting method, taking into account the influence of the verticality and bending stiffness of the suspender, the formula is applied to the actual project, and good results are obtained. Gaute-Alonso et al. [26] used a force-measuring sensor, unidirectional strain gauge, and vibration wire technology based on an accelerometer to monitor cable force, and evaluated the advantages and disadvantages of different technologies. In addition, according to the comparison between the measured data and the theoretical calculation data of the finite element method, it is found that the effect of temperature on the beam-arch composite system bridge cannot be ignored [27,28]. Mei et al. [29] studied the response characteristics of the steel box girder of a long-span cable-stayed bridge under sunlight temperatures based on temperature monitoring during construction. The process of bridge design will comprehensively consider the actual construction as much as possible. However, in bridge construction, non-human factors and construction errors are difficult to avoid completely. Therefore, in this case, it is usually necessary to focus on the real-time monitoring of the whole construction process, and the construction monitoring technology of reasonable adjustment and improvement in the construction process came into being [30,31].

Bridge construction monitoring is becoming increasingly important. In this paper, based on the newly built Dafeng River Bridge in the reconstruction and expansion project of the Qinzhou–Beihai Section of the Lanhai Expressway in Guangxi Province, which belongs to the bowstring type, the construction monitoring research is carried out through rigid frame tied steel box arch bridge. MIDAS Civil finite element software is used for the symmetrical construction monitoring simulation to calculate the deformation and stress of the tied steel box arch bridge at the construction and completion stages. Through the finite element calculation analysis, the deviation state of the bridge during construction can be controlled and adjusted to ensure that the stress and linear state of the bridge under the completed state meet the requirements. Finally, according to the measured and theoretical calculation results, the completed state of the newly built Dafeng River Bridge under symmetrical construction monitoring can be evaluated to check whether it conforms to the design state. According to the actual engineering, the simulation and monitoring results can be used to verify the finite element model and guide the actual construction.

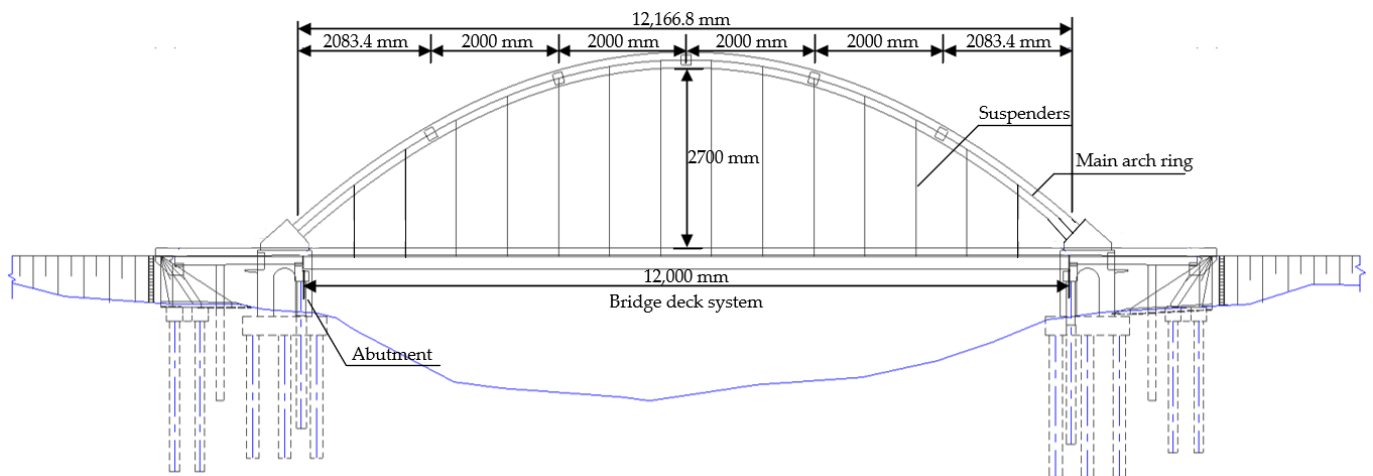
## 2. Project Overview

### 2.1. Bridge Overview

In this study, a bridge located in Qinzhou City crossing the Dafeng River is selected, which belongs to the reconstruction and expansion project of the Qinzhou–Beihai Section of the Lanhai Expressway. Without changing its existing navigation, the upper part and bent cap of the existing bridge were demolished and rebuilt as the left part of the whole bridge after reconstruction. The right part is the newly built Dafeng River Bridge on the downstream side, which is a tied-through-rigid-frame steel box arch bridge. The appearance of the reconstructed whole bridge is shown in Figure 1a.



(a)



(b)

**Figure 1.** The newly built Dafeng River Bridge: (a) appearance; (b) elevation layout.

The newly built Dafeng River Bridge has a clear span of 120.0 m, a clear rise of 27.0 m, and a clear rise-to-span ratio of 1/4.44, which provides a beautiful appearance, strong crossing ability, and reasonable stress performance. The elevation layout of the newly built Dafeng River Bridge is shown in Figure 1b. The arch's camber is 15.0 cm, and the arch axis adopts a secondary parabola. The main arch rib is a single box and single room steel box section with equal sections, the section height is 2.50 m, and the width is 1.80 m. The main bridge is a one-span main arch with two arch ribs. A total of five lateral braces are set between the two arch ribs to ensure the overall stability of the arch bridge. The lateral brace is a steel box structure with a horizontal length of 24.30 m, a square section, and a height and width of 1.52 m. The thickness of the top, bottom, and web

of the cross brace is 20 mm. In addition, the suspender adopts a GJ15-27 whole bundle of extruded steel strand suspenders, with a spacing of 26.1 m in the transverse direction and 8.0 m in the longitudinal direction. There are 14 pairs of suspenders in the whole bridge. The XGK-II 15–31 full anti-corrosion full bundle-replaceable adjustable high-strength low-relaxation steel strand finished cable is used. Additionally, eight tie rod tensioning holes are arranged under each arch rib, including six permanent tie rods and two reserved cable replacement holes. The bridge deck system is a steel lattice system, which is composed of steel longitudinal beams, main beams, secondary beams, and steel–concrete composite bridge decks. For the bridge deck, an 8 mm thick steel plate is welded on the beam grid as the bottom formwork, and 15 cm thick C40 steel fiber concrete is cast in situ. The bridge deck is paved with 7 cm asphalt concrete. The main pier is the solid pier, cushion cap, and pile foundation, and the main bridge cushion cap, main pier, and arch abutment are all poured with large-volume concrete.

## 2.2. Finite Element Model of the Newly Built Dafeng River Bridge

For construction monitoring of the newly built Dafeng River bridge, the finite element simulation calculation should be carried out first. MIDAS Civil 2019 is used to carry out the calculation of each construction stage, including the stress of each section and the theoretical alignment of construction control. The finite element calculation results are used as the basis for the alignment and stress control at each stage of construction monitoring.

The main material parameters of the finite element model of the newly built Dafeng River Bridge are shown in Table 1. Q355C is used as an arch rib, transverse brace, and lattice beam, and Q235C is used as a steel deck. C40, C35, and C50 are used for the main pier, deck, sidewalk and access slab, cushion cap concrete, and arch abutment concrete.  $\varphi^s15.24$  is adopted as a suspender and tie rod. The permanent load mainly includes the dead weight of steel and concrete, referring to Table 1. Asphalt bridge deck pavement, anti-collision guardrail, handrail, tie box, and other structures are considered loads. The deck pavement load is  $0.07 \times 24 = 1.68 \text{ kN/m}^2$ . The anti-collision guardrail is applied according to the beam unit load, and the value is 9.5 kN/m. The sidewalk slab and handrail are applied according to the pressure load, and the value is 6.0 kN/m<sup>2</sup>. The access slab is applied according to the pressure load, and the value is 10.0 kN/m<sup>2</sup>. The shrinkage and creep of concrete shall be calculated according to the relevant provisions of JTG 3362-2018. The tie rods are tensioned two times. The first tensioning control force is 1400 kN, the second tensioning control force of tie rods N2~N8 is 2200 kN, and the tensioning control force of tie rods N10~N16 is 2250 kN.

**Table 1.** The main material parameters of the finite element model.

No.	Material	Elastic Modulus	Linear Expansion Coefficient	Unit Weight
1	Q355C	$2.06 \times 10^5$	$1.20 \times 10^{-5}$	76.98
2	Q235C	$2.06 \times 10^5$	$1.20 \times 10^{-5}$	76.98
3	C40	$3.25 \times 10^4$	$1.00 \times 10^{-5}$	26.00
4	C35	$3.15 \times 10^4$	$1.00 \times 10^{-5}$	26.00
5	C50	$3.45 \times 10^4$	$1.00 \times 10^{-5}$	26.00
6	$\varphi^s15.24$	$1.90 \times 10^5$	$1.20 \times 10^{-5}$	78.50

Then, for the finite element model of the newly built Dafeng River Bridge, the lattice beam, arch rib, and transverse brace are simulated by beam element, the suspender and tie bar are simulated by truss element, and the deck steel bottom plate, the bridge deck plate, sidewalk plate, and access slab are simulated by plate element. At the same time, the shrinkage and creep effects of concrete in the construction stage are considered. The structural schematic diagram of the key construction stages of the newly built Dafeng River Bridge is shown in Figure 2 when the lattice beam is assembled at the completion stage.

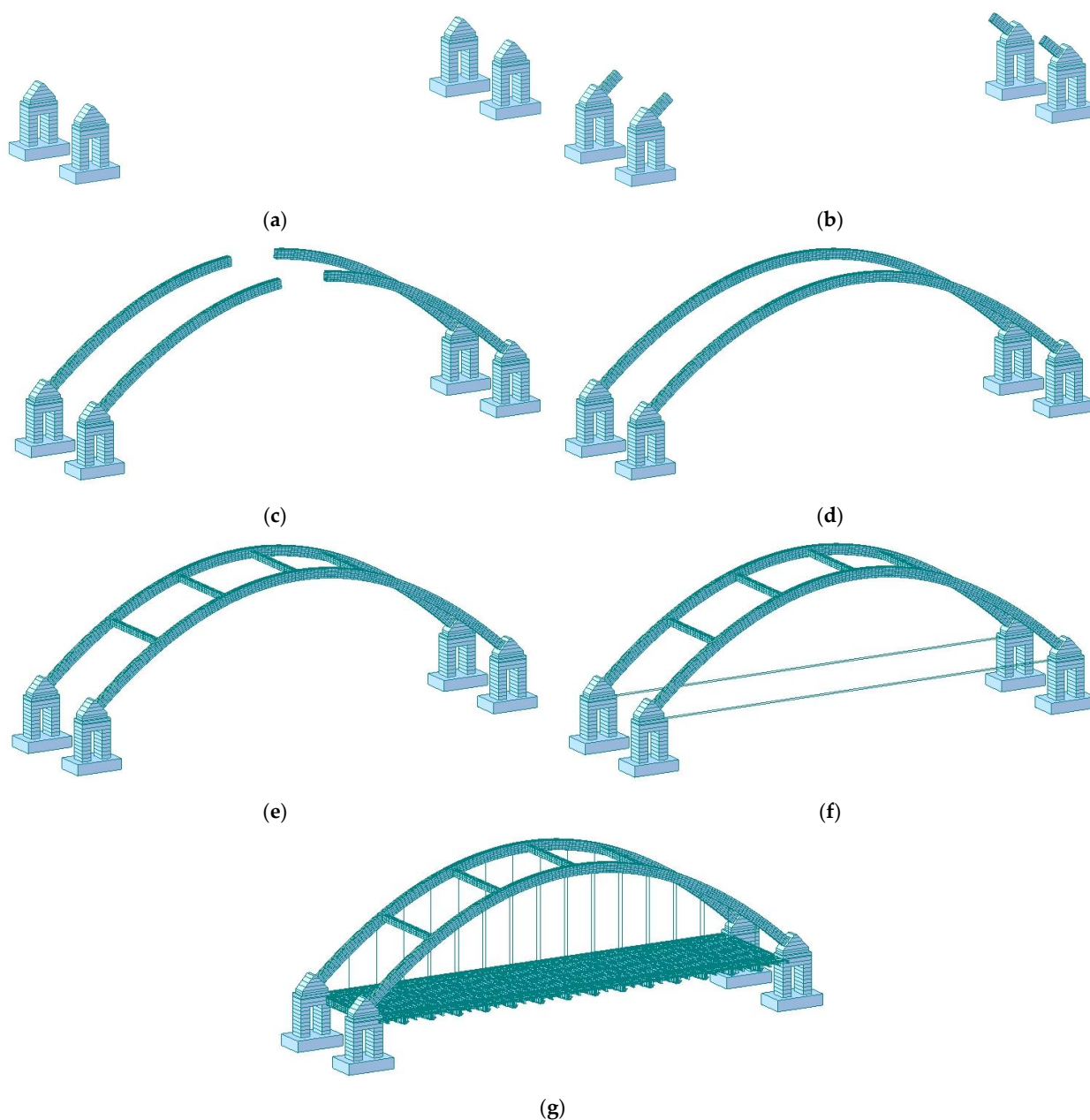


**Figure 2.** The structural schematic diagram of the key construction stages: (a) arch abutment construction completed; (b) arch rib section 1 installation completed; (c) arch rib section 4 installation completed; (d) arch rib closure; (e) transverse brace installation completed; (f) remove the arch rib bracket and tension the tie bar; and (g) construction completion.

### 3. Results and Discussion

#### 3.1. Finite Element Calculation and Analysis in Bridge Construction Stage

##### 3.1.1. Stress Calculation Results and Analysis

Structural stress is an important content of construction monitoring, which can judge the stress state of the bridge and play an early warning role for the safety of the bridge. The structural stress should be kept within a reasonable allowable range. Too large or too small an amount of structural stress is harmful to the safety of the structure. If the amount of stress is too large, the concrete compressive stress exceeds the limit value of its compressive bearing capacity, and the concrete is damaged. If the amount of structural stress is too small, part of the concrete will be subject to tensile stress, and cracks will also affect the safety of the bridge.

### 1. Stress of Main Arch and Transverse Brace during Construction

The finite element simulation model of the tied steel box arch bridge is established, as shown in Figure 2. The finite element model is calculated to obtain the stress value of the box girder of the upper structure of the main bridge at the construction stage, and the theoretical calculation analysis is carried out. The tensile stress and compressive stress of the superstructure of the main bridge (including the main arch and transverse brace) of the newly built Dafeng River Bridge during construction are shown in Figure 3. As seen in Figure 3, the tensile stress and compressive stress of the main arch and transverse brace of the main bridge are symmetrically distributed. The maximum tensile stress of the main arch and transverse brace is 15.1 MPa (from Figure 3a), and the maximum compressive stress of the main arch and transverse brace is 74.6 MPa (from Figure 3b). The maximum tensile and compressive stress values are less than  $(270/1.1 = 245.5)$  MPa allowed by the specification, and the main arch and transverse brace meet the specification requirements at the construction stage.

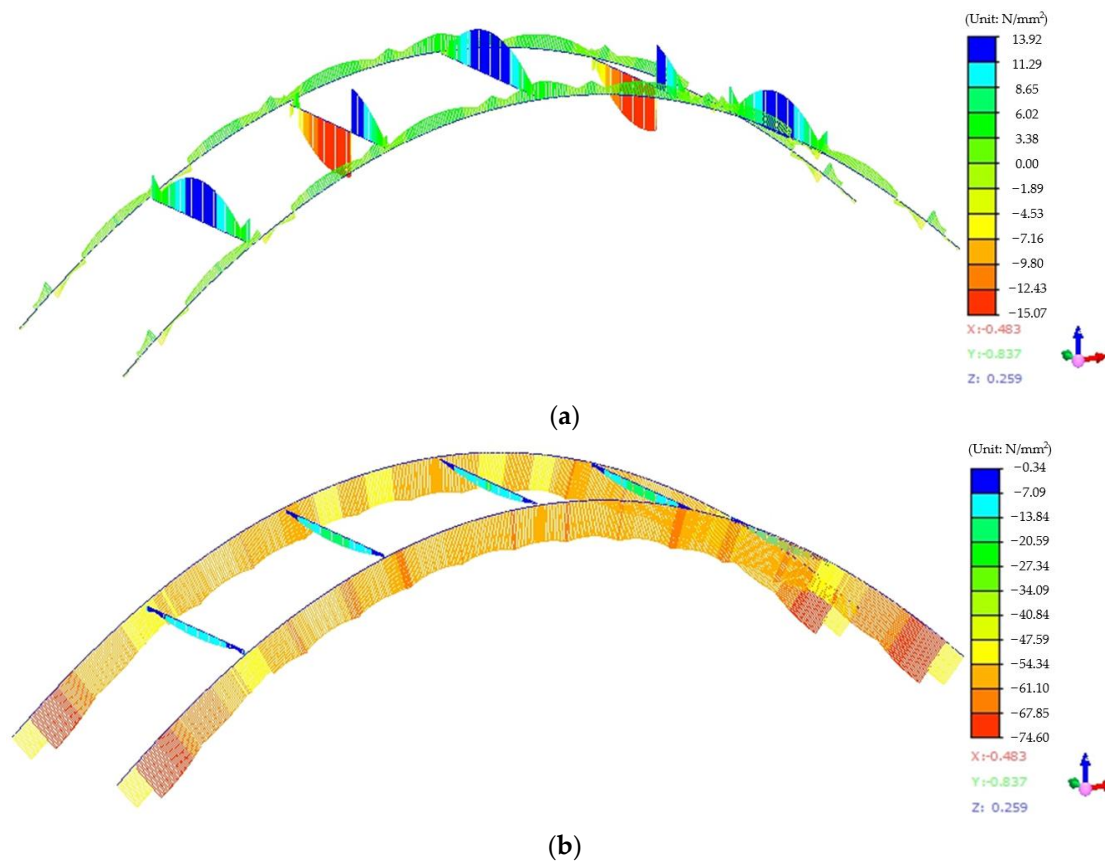


**Figure 3.** The maximum tensile and compressive stress of the main arch and transverse brace during the construction of the newly built Dafeng River Bridge: (a) maximum tensile stress; (b) maximum compressive stress.

### 2. Stress of Lattice Beam during Construction

The finite element model is calculated to obtain the stress value of the lattice beam of the main bridge at the construction stage, and the theoretical calculation analysis is also carried out. The tensile stress and compressive stress of the lattice beam of the main bridge of the newly built Dafeng River Bridge during construction are shown in Figure 4. The tensile stress and compressive stress of the lattice beam are symmetrically distributed. Figure 4a shows that the maximum tensile stress of the lattice beam is 11.9 MPa, and Figure 4b shows that the maximum compressive stress of the lattice beam is 81.5 MPa. The

maximum tensile and compressive stress values are less than the 245.5 MPa allowed by the specification, meeting the specification requirements at the construction stage.

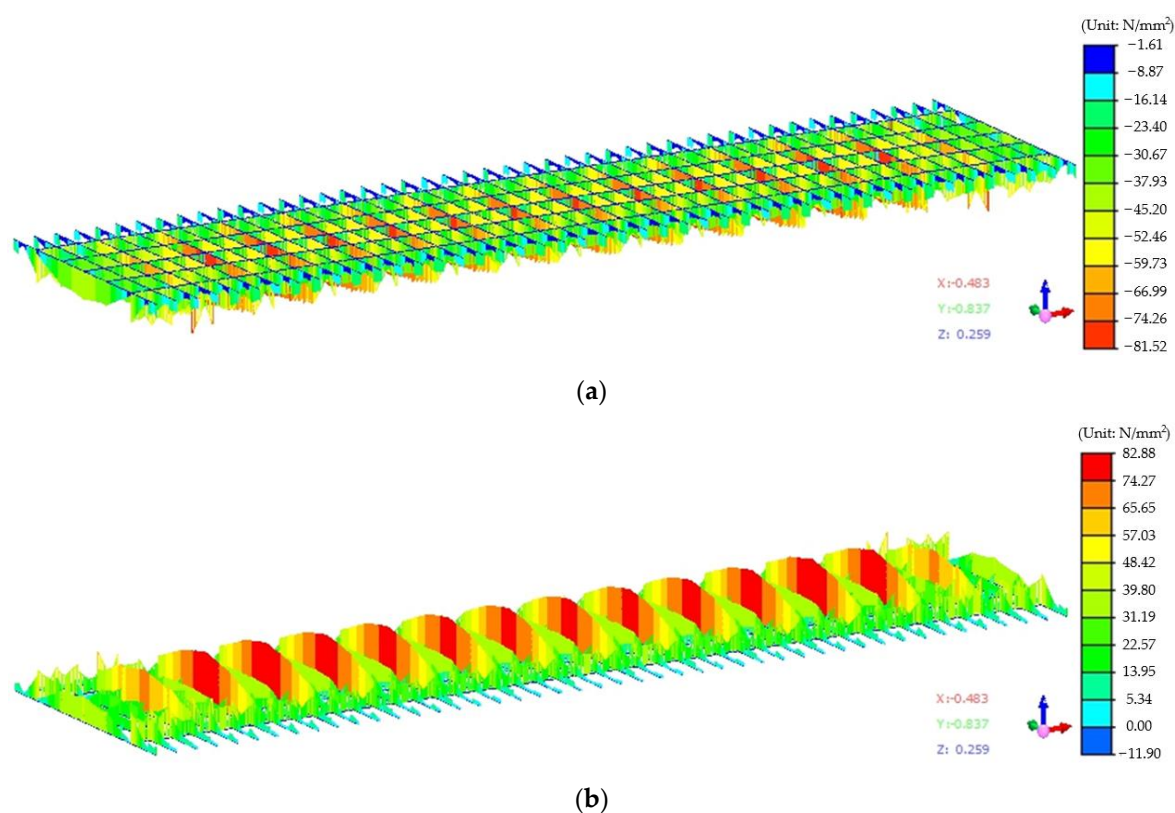


**Figure 4.** The maximum tensile and compressive stress of the lattice beam during the construction of the newly built Dafeng River Bridge: (a) maximum tensile stress; (b) maximum compressive stress.

### 3.2. Displacement Calculation Results and Analysis

Due to many working conditions, only the key working condition after the completion of Phase II construction and the secondary tensioning of tie bars is selected for the displacement and deformation analysis of the main arch and lattice beam of the main bridge of the newly built Dafeng River Bridge. The finite element model shown in Figure 2g is selected and calculated to obtain the displacement value of the main arch and lattice beam of the main bridge at the construction stage, and the theoretical calculation analysis is carried out. The cumulative displacement of the main arch and lattice beam of the main bridge of the newly built Dafeng River Bridge during construction is shown in Figure 5. It can be seen that the cumulative displacement of the main arch and lattice beam of the main bridge are symmetrically distributed. In addition, it can be seen from Figure 5a,b that after the supports are removed, the secondary dead load is arranged, and the cable force of the suspender is adjusted, the cumulative displacement of the main arch and lattice beam at the midspan is the largest. Therefore, in online shape monitoring, it is necessary to pay close attention to the displacement change and development trend, compare the theoretical value of the model to correct the monitoring error, and reasonably adjust the construction.

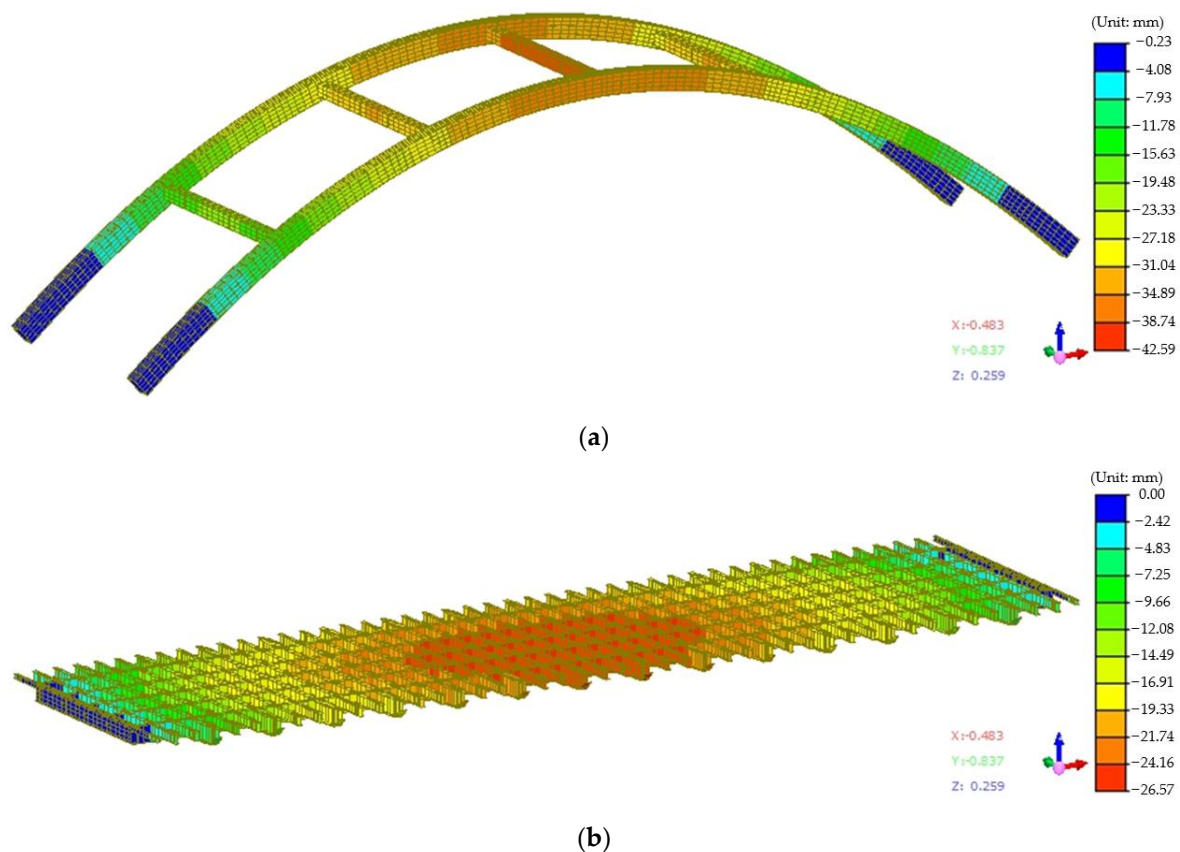


**Figure 5.** The cumulative displacement of the main arch and lattice beam of the main bridge during the construction of the newly built Dafeng River Bridge: (a) cumulative displacement of the main arch; (b) cumulative displacement of the lattice beam.

#### 4. Finite Element Structural Checking Calculation in Bridge Completion Stage

##### 4.1. Force Calculation Results and Analysis

According to the construction scheme design of the newly built Dafeng River Bridge, the bridge completion stage is the working condition after the completion of Phase II construction and the secondary tensioning, and the finite element model in the bridge completion stage is shown in Figure 2g. After the completion of the newly built Dafeng River Bridge, the force of the main arch and transverse brace, the force of the lattice beam, and the cable force of the suspender of the newly built Dafeng River Bridge are shown in Figures 6–8, respectively, including bending moment, axial force and shear force.

It can be seen from Figure 6a that after the completion of the newly built Dafeng River Bridge, the bending moment of the main arch is generally symmetrically distributed, and the variation is relatively uniform. The maximum bending moment occurs at the junction of the main arch and lattice beam. The bending moment of the transverse brace is also distributed symmetrically with a relatively uniform degree. It can be seen from Figure 6b that the axial force under the completed bridge is in the compression state as a whole and is symmetrically distributed. The overall distribution of the axial force is gradually decreasing from the junction of the arch beam to the middle. It can be seen from Figure 6c that compared with the bending moment diagram, the shear force in the completed bridge is distributed symmetrically. In addition, after the completion of the newly built Dafeng River Bridge, the bending moment, axial force, and shear force of the lattice beam, as well as the suspender cable force, are generally symmetrically distributed. The change in internal force is relatively uniform, and the maximum bending moment appears on both sides of the lattice beam. The overall distribution is gradually decreasing from the middle to both sides.

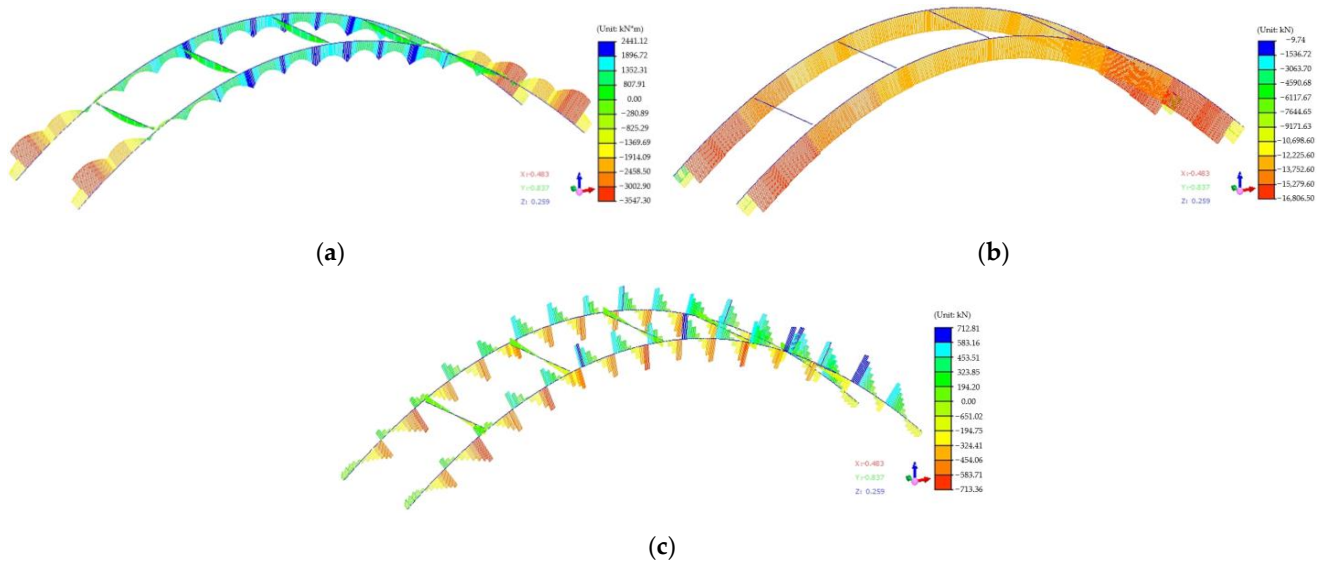


Figure 6. The force of main arch and transverse brace after the completion of the newly built Dafeng River Bridge: (a) bending moment diagram; (b) axial force diagram; and (c) shear force diagram.

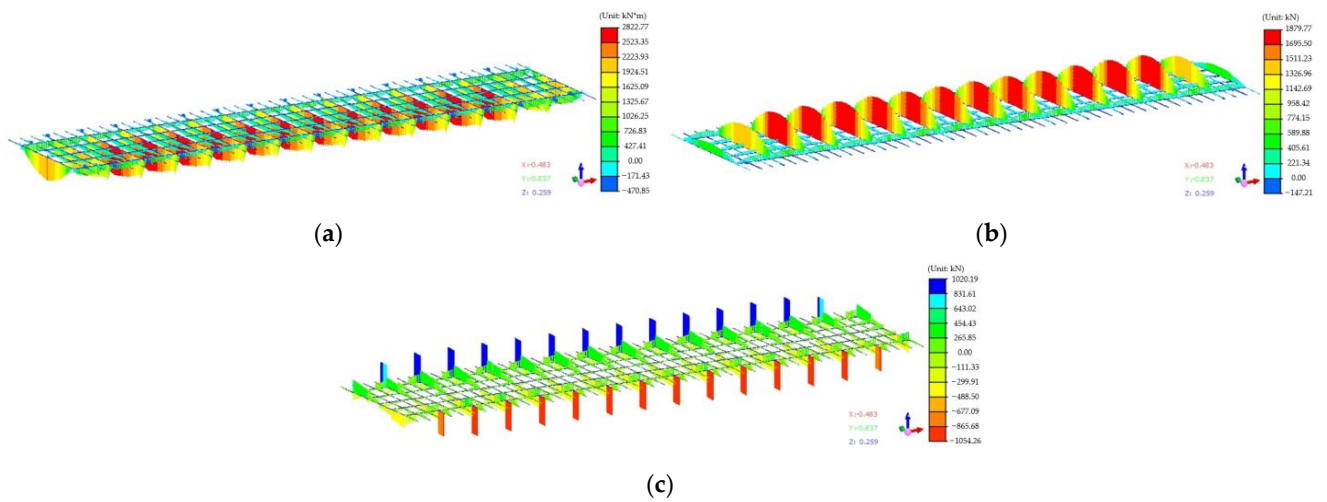


Figure 7. The force of lattice beam after the completion of the newly built Dafeng River Bridge: (a) bending moment diagram; (b) axial force diagram; and (c) shear force diagram.

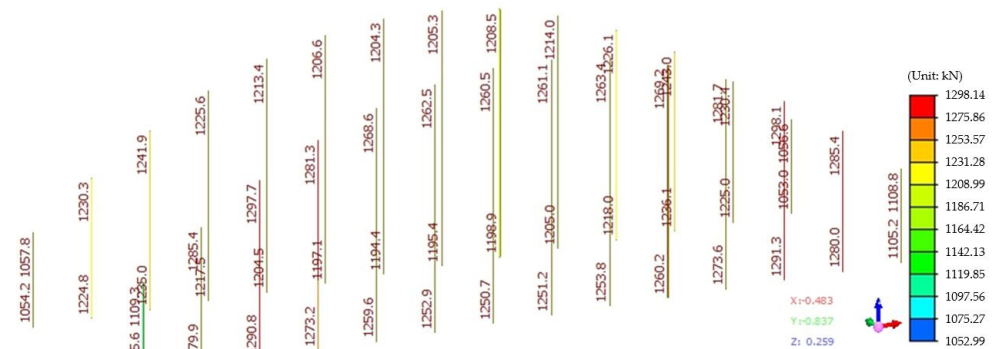


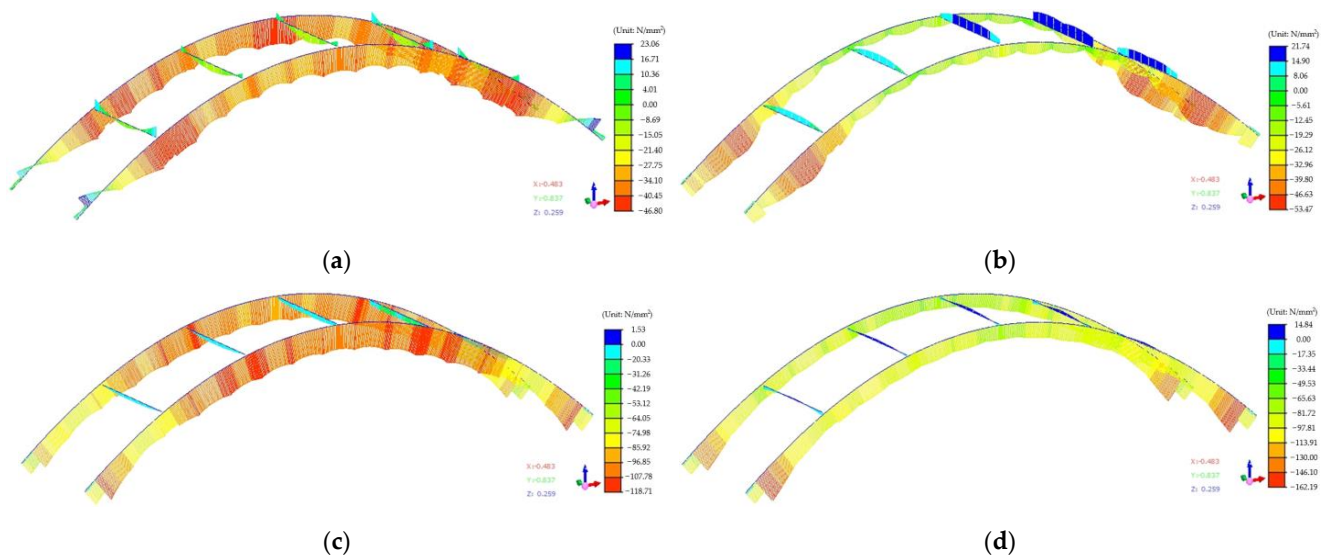
Figure 8. The cable force of the suspender after the completion of the newly built Dafeng River Bridge.

#### 4.2. Structural Checking Calculation Results

Subsequently, the load combination of the newly built Dafeng River Bridge is carried out in this study, and the stress of the main components (including the main arch, transverse brace and lattice beam, suspender, and tie rod) of the newly built Dafeng River Bridge under different load combinations during the operation stage of the completed bridge is calculated, and checked by the current specifications. Since the main bridge of the newly built Dafeng River Bridge is on the expressway, the structural importance coefficient is 1.1. According to the Chinese specification “General Specifications for Design of Highway Bridges and Culverts” (JTG D60-2015), the ultimate limit state of bearing capacity and serviceability limit state are checked in this study. The variable load mainly considers vehicle load, crowd load, system temperature load, temperature gradient load, steel tension, shrinkage and creep, etc., which can generate different load combinations for the ultimate limit state of bearing capacity and the serviceability limit state. When the highway bridge and culvert structure is designed according to the ultimate limit state of bearing capacity, the basic combination is adopted for the permanent design condition and the temporary design condition. When the highway bridge and culvert structure is designed according to the serviceability limit state, two kinds of action–effect combinations are adopted, i.e., the frequency combination of action and the quasi-permanent combination.

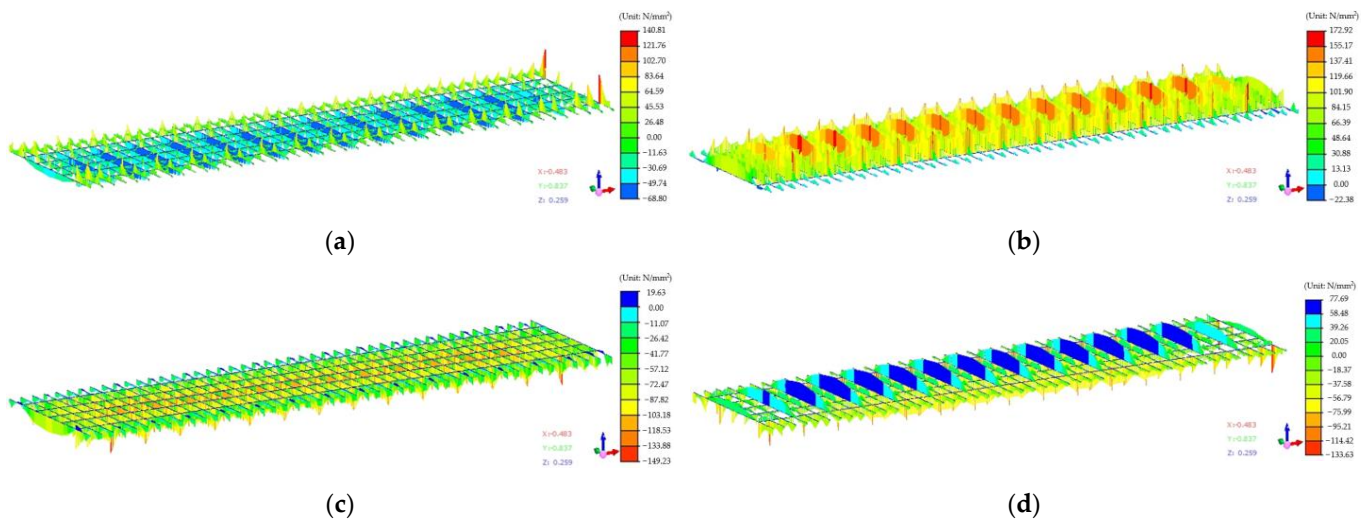
##### 1. Structural Checking of Main Arch, Transverse Brace, and Lattice Beam

Figure 9 shows the structural checking calculation results of the main arch and transverse brace of the newly built Dafeng River Bridge under the ultimate limit state of bearing capacity. The maximum tensile stress envelope diagram of the main arch and transverse brace on both top and bottom surfaces are plotted in Figure 9a,b, and the maximum compressive stress envelope diagram of the main arch and transverse brace on both top and bottom surfaces are plotted in Figure 9c,d. It can be seen that under basic combinations of the ultimate limit state of bearing capacity, the stress of the main arch and transverse brace on the top surface is between  $-118.7$  MPa and  $23.1$  MPa, and the stress on the bottom surface is between  $-162.2$  MPa and  $21.7$  MPa, both of which are less than the  $(270/1.1 = 245.5)$  MPa allowed by the specification, meeting the specification requirements.



**Figure 9.** The maximum tensile and compressive stress envelope diagram of main arch and transverse brace under basic combinations of ultimate limit state of bearing capacity: (a) envelope diagram of maximum tensile stress on top surface; (b) envelope diagram of maximum tensile stress on bottom surface; (c) envelope diagram of maximum compressive stress on top surface; and (d) envelope diagram of maximum compressive stress on bottom surface.

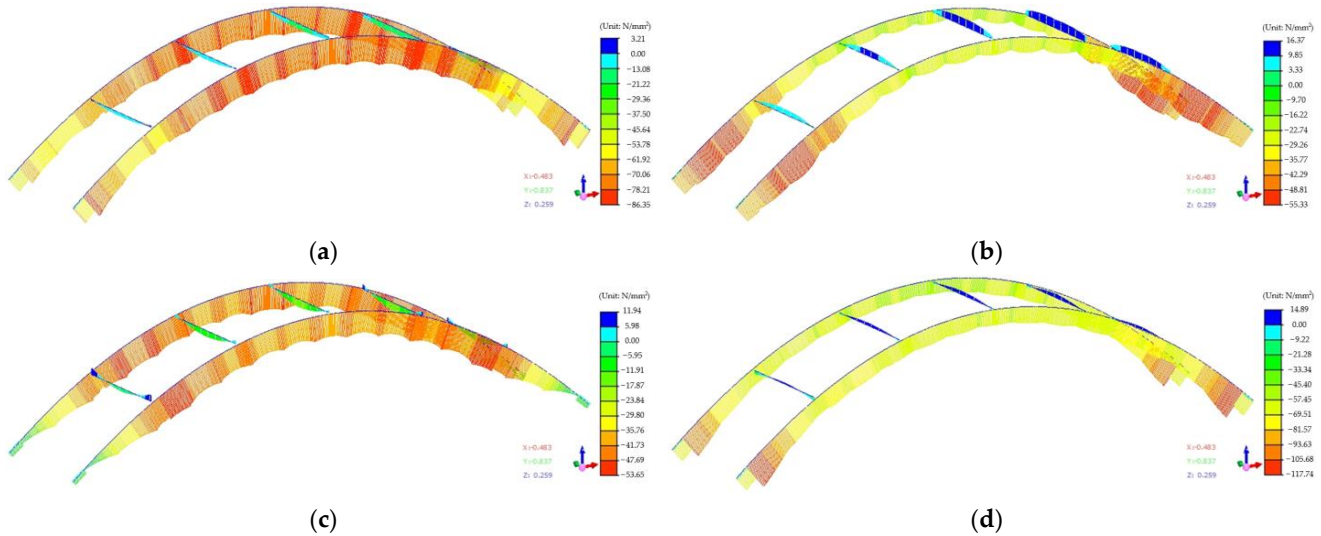
Under basic combinations of the ultimate limit state of bearing capacity, the maximum tensile stress envelope diagram of the lattice beam on both top and bottom surfaces are plotted in Figure 10a,b, respectively, and Figure 10c,d show the maximum compressive stress envelope diagram of lattice beam on both top and bottom surfaces. It can be seen that under basic combinations of the ultimate limit state of bearing capacity, the stress of the lattice beam on the top surface is between  $-149.2$  MPa and  $140.8$  MPa, and the stress on the bottom surface is between  $-133.6$  MPa and  $172.9$  MPa, both of which are less than the  $245.5$  MPa allowed by the specification, meeting the specification requirements.



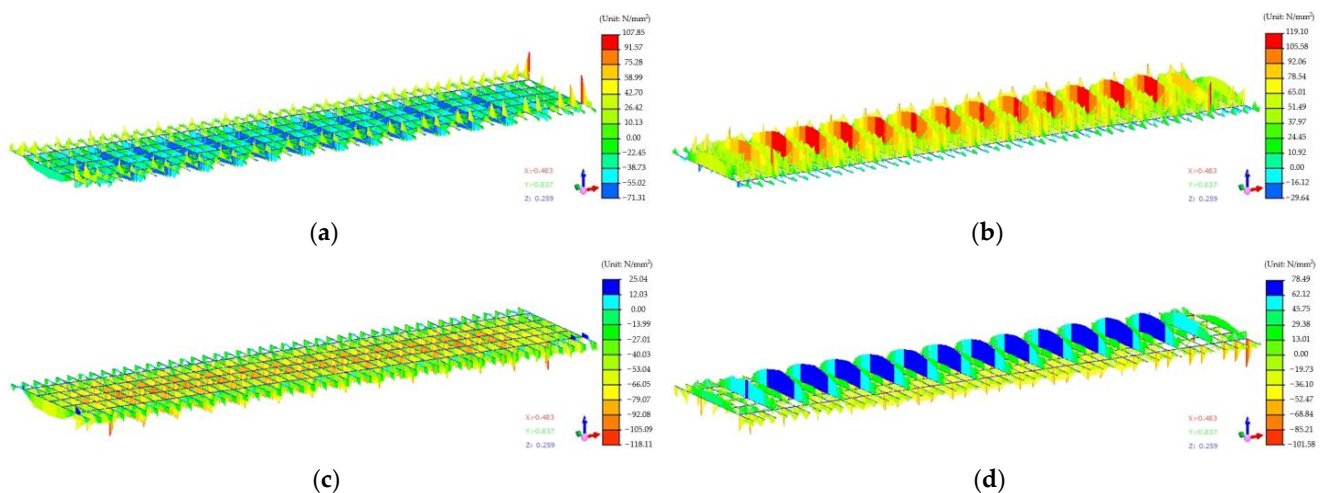
**Figure 10.** The maximum tensile and compressive stress envelope diagram of lattice beam under basic combinations of ultimate limit state of bearing capacity: (a) envelope diagram of maximum tensile stress on top surface; (b) envelope diagram of maximum tensile stress on bottom surface; (c) envelope diagram of maximum compressive stress on top surface; and (d) envelope diagram of maximum compressive stress on the bottom surface.

Figure 11 shows the structural checking calculation results of the main arch and transverse brace of the newly built Dafeng River Bridge under the serviceability limit state. The maximum tensile stress envelope diagram of the main arch and transverse brace on both top and bottom surfaces under the serviceability limit state is plotted in Figure 11a,b. Additionally, the maximum compressive stress envelope diagram of the main arch and transverse brace on both top and bottom surfaces under the serviceability limit state is plotted in Figure 11c,d. It can be seen that under loading combinations of the serviceability limit state, the stress of the main arch and transverse brace on the top surface is between  $-53.7$  MPa and  $3.2$  MPa, and the stress on the bottom surface is between  $-117.8$  MPa and  $16.4$  MPa, both of which are less than the  $245.5$  MPa allowed by the specification, meeting the specification requirements.

The maximum tensile stress envelope diagram of the lattice beam on both top and bottom surfaces under basic combinations of serviceability limit state is plotted in Figure 12a,b, respectively, and Figure 12c,d show the corresponding maximum compressive stress envelope diagram of the lattice beam on both top and bottom surfaces. It can be seen that under basic combinations of serviceability limit state, the stress of the lattice beam on the top surface is between  $-118.1$  MPa and  $107.9$  MPa, and the stress on the bottom surface is between  $-101.6$  MPa and  $119.1$  MPa, both of which are less than the  $245.5$  MPa allowed by the specification, meeting the specification requirements.



**Figure 11.** The maximum tensile and compressive stress envelope diagram of main arch and transverse brace under basic combinations of serviceability limit state: (a) envelope diagram of maximum tensile stress on top surface; (b) envelope diagram of maximum tensile stress on bottom surface; (c) envelope diagram of maximum compressive stress on top surface; and (d) envelope diagram of maximum compressive stress on bottom surface.



**Figure 12.** The maximum tensile and compressive stress envelope diagram of lattice beam under basic combinations of serviceability limit state: (a) envelope diagram of maximum tensile stress on top surface; (b) envelope diagram of maximum tensile stress on bottom surface; (c) envelope diagram of maximum compressive stress on top surface; and (d) envelope diagram of maximum compressive stress on the bottom surface.

## 2. Structural Checking of Suspender and Tie Rod

Figure 13a shows the cable force results of the suspender of the main bridge of the newly built Dafeng River Bridge under the ultimate limit state of bearing capacity. It can be seen from Figure 13a that the maximum cable force of the suspender of the main bridge for the newly built Dafeng River Bridge under the ultimate limit state of bearing capacity is 2189.4 kN. The type of the suspender adopted for the main bridge of the newly built Dafeng River Bridge is GJ15-27, the corresponding breaking cable force is 7020 kN, and the minimum safety factor of the suspender of the whole bridge is  $(7020/2189.4) = 3.2$ . According to the Chinese specification “Specifications for Design of Highway Concrete-filled Steel Tubular Arch Bridges” (JTG D65-06-2015), the safety factor of steel strand

suspenders under permanent state shall not be less than 2.5. Therefore, the minimum safety factor of the suspender of the whole bridge (i.e., 3.2) is larger than the 2.5 specified, meeting the specification requirements.

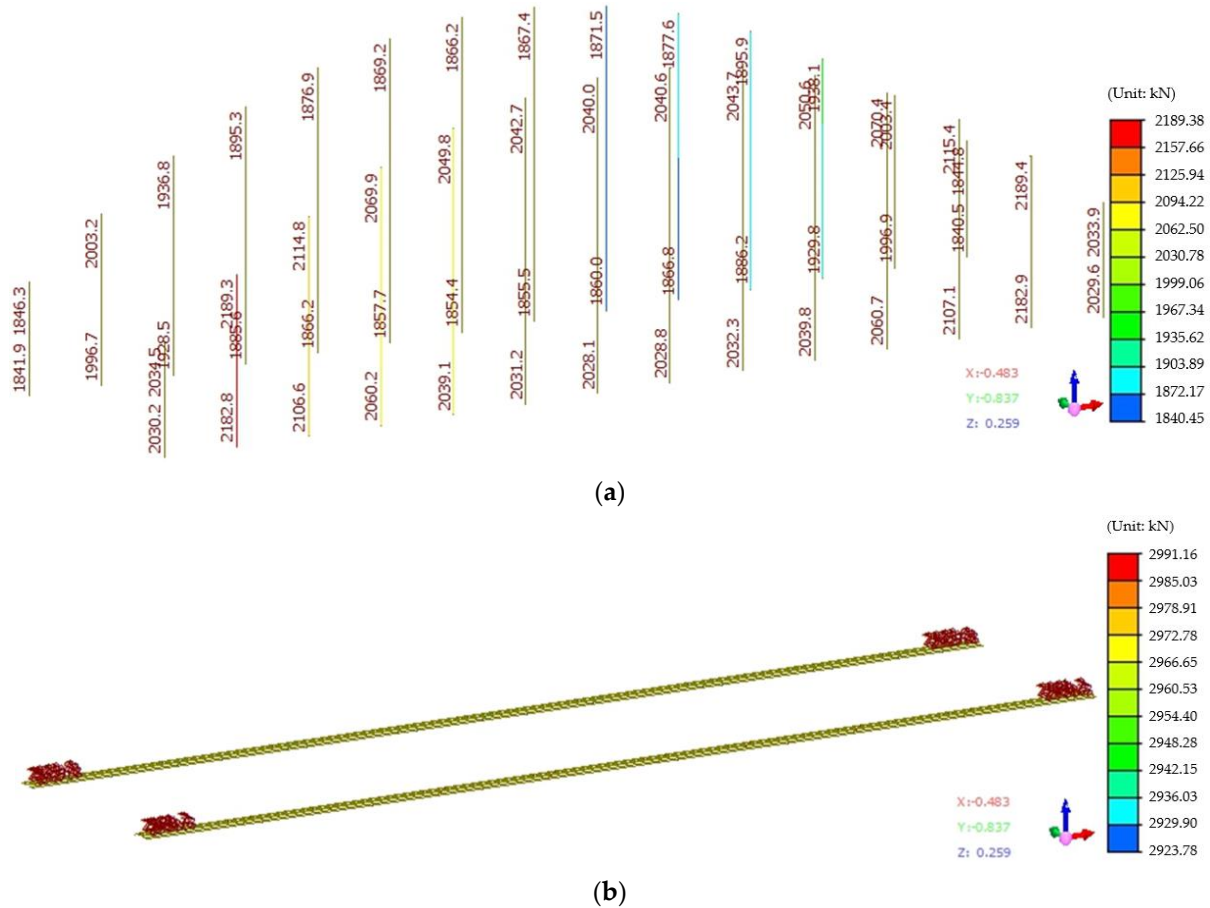


**Figure 13.** The cable forces of the newly built Dafeng River Bridge under basic combinations of ultimate limit state of bearing capacity: (a) suspender; and (b) tie rod.

The cable force results of the tie rod of the main bridge of the newly built Dafeng River Bridge under the ultimate limit state of bearing capacity are shown in Figure 13b. It can be seen from Figure 13b that the maximum cable force of the tie rod of the main bridge for the newly built Dafeng River Bridge under the ultimate limit state of bearing capacity is 2991.2 kN. The type of the tie rod adopted for the main bridge of the newly built Dafeng River Bridge is GJ15-31, the corresponding breaking cable force is 8072.4 kN, and the minimum safety factor of the tie rod of the whole bridge is  $(8072.4/2991.2) = 2.7$ . According to the Chinese specification “Specifications for Design of Highway Concrete-filled Steel Tubular Arch Bridges” (JTG D65-06-2015), the safety factor of steel strand tie rods under permanent state shall not be less than 2.0. Therefore, the minimum safety factor of the tie rod of the whole bridge (i.e., 2.7) is larger than the 2.0 specified, meeting the specification requirements.

### 5. Analysis of Camber of Arch and Lattice Beam, Blanking Length of Suspender

#### 1. Camber Calculation of Arch and Lattice Beam

The camber is set to offset the deflection of the main beam under load. The setting of the camber can be reversed according to the accumulated deflection after shrinkage and creep. In this study, the camber of the main arch and lattice beam is calculated as Equation (1):

$$\text{Camber} = D_{dead} + 0.5 \times D_{vehicle} + D_{construction} + SC_{10} \tag{1}$$

in which  $D_{dead}$  is the dead load displacement,  $D_{vehicle}$  is the load displacement,  $D_{construction}$  is the construction load displacement, and  $SC_{10}$  is 10 years of shrinkage creep.

The camber of the main arch and lattice beam of the main bridge for the newly built Dafeng River Bridge is determined through the finite element simulation calculation, taking into account the dead load, live load, construction load, and shrinkage creep in Equation (1), which is used to guide the subsequent construction. The camber calculation results of the main arch and lattice beam of the main bridge for the newly built Dafeng River Bridge are summarized in Figure 14a,b, respectively. In the calculation results, the calculation of the camber does not include the deformation of the steel platform. As seen in Figure 14a,b, the maximum calculated camber value of the main arch is 19.3 cm, and the maximum calculated camber value of the lattice beam is 21.7 cm.

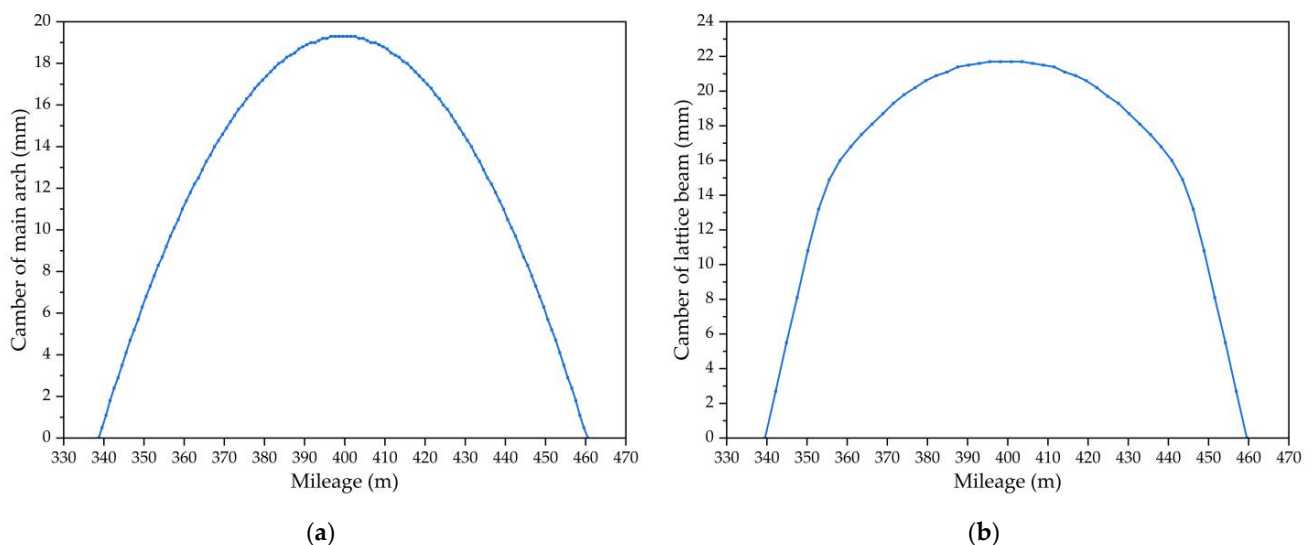


**Figure 14.** The camber calculation results of the main bridge for the newly built Dafeng River Bridge: (a) main arch; and (b) lattice beam.

## 2. Calculation of Blanking Length of Suspender

The lattice beam is suspended on the main arch by the suspender, and the length of the suspender will directly affect the alignment of the bridge. The stress-free length of the suspender will be accurately calculated to ensure that the stress of the whole bridge meets the design requirements, and also to ensure the beauty of the bridge. The blanking length of the suspender is the length of the suspender under the state of no stress, and the difference between the deflection of the arch rib (caused by the deformation of the support, the secondary dead load, and other factors), the elastic elongation of the suspender, the designed camber, and the actual deformation of the main arch rib is deducted. In this study, the finite element software MIDAS Civil 2019 is used to calculate and analyze the unstressed length of the suspender, and the length of the suspender under the unstressed state can be obtained, that is, the blanking length of the suspender. The blanking length results of the upstream and downstream suspenders calculated by the finite element method are shown in Figure 15. Figure 15 shows the blanking length of each suspender on both sides of the upstream and downstream. It can be seen that the blanking length of the suspender is symmetrically distributed from both sides of the upstream and downstream as well as both rivers. The exact length of each suspender is calculated separately, which is of great guiding significance for construction.

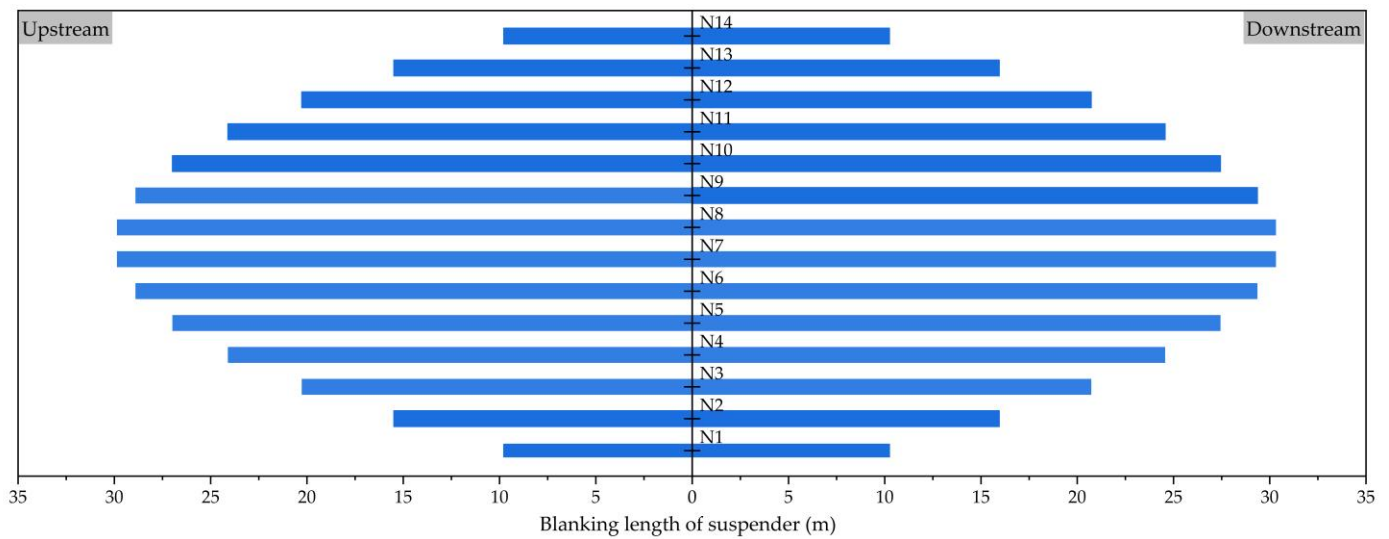
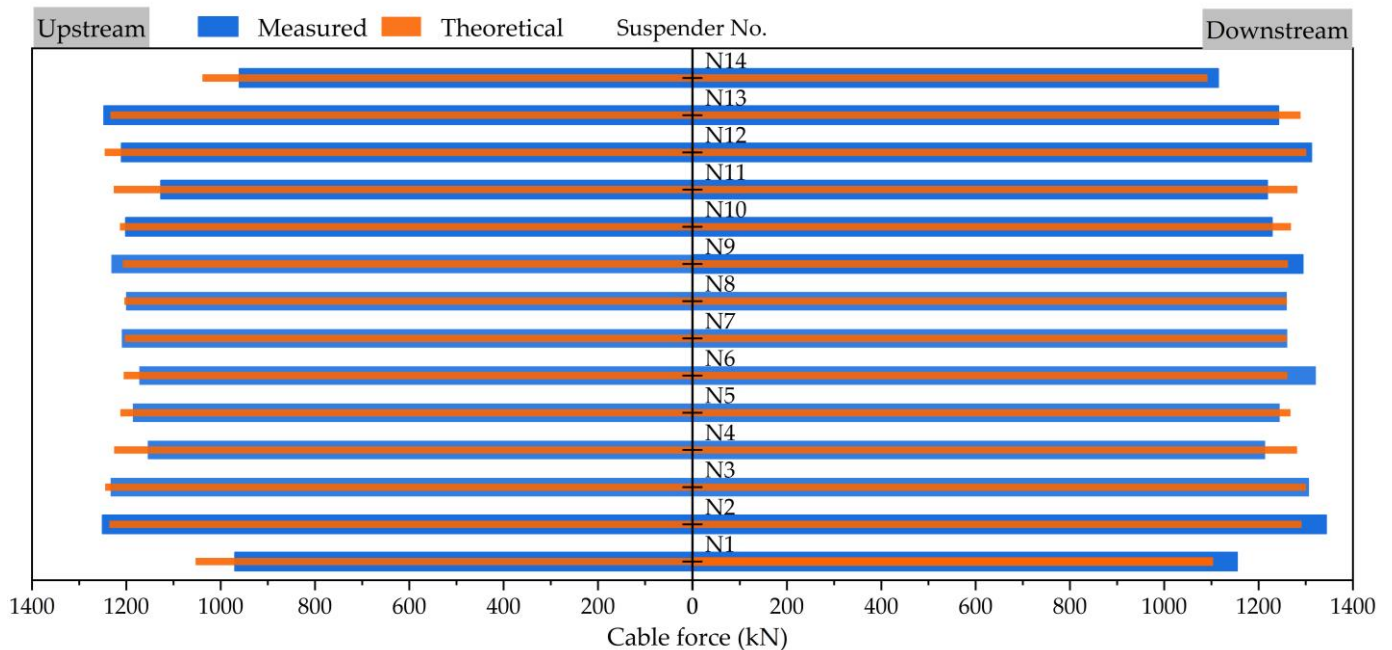


**Figure 15.** The blanking length results from the upstream and downstream suspenders.

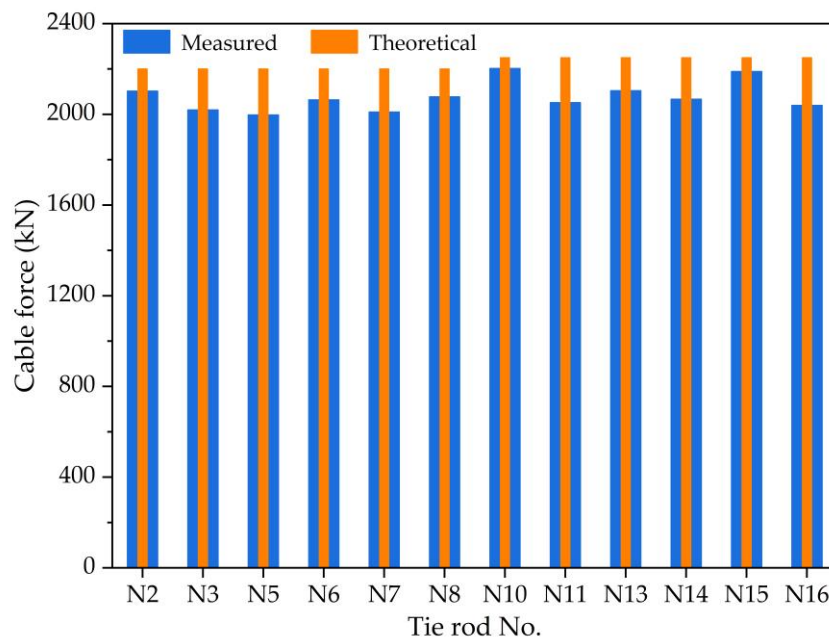
## 6. Comparative Analysis and Evaluation of Alignment and Cable Force after Bridge Construction Completion

The cable forces of the suspender and tie rod are important design parameters, which are also important construction monitoring parameters to be controlled. The measurement effect and accuracy of cable force will directly affect the construction quality and status of the bridge structure. There are 14 pairs of suspenders in the whole bridge, including the upstream and downstream. Additionally, there is eight tie rod tensioning holes under the arch rib, including six permanent tie rods and two reserved cable replacement holes. Therefore, after the completion of the bridge deck pavement (that is the last process of bridge construction), the on-site test and finite element model calculation analysis of cable force for 28 suspenders and 12 tie rods of the whole bridge were carried out before the whole bridge was opened to traffic. The comparison between the measured values and the theoretical values of the suspender cable force is shown in Figure 16a. The comparison between the measured values and the theoretical values of the tie rod cable force is shown in Figure 16b. It can be seen from Figure 16 that the deviation values between the on-site measurement and theoretical calculation of the cable forces of the suspender and tie rod are within 10%, meeting the deviation of  $\pm 10\%$  required in “Inspection and Evaluation Quality Standards for Highway Engineering” (JTG F80/1-2017). The alignment is one of the most important feedback indicators in structural construction monitoring. The measuring points of the bridge deck alignment after the completion of the bridge are arranged on the bridge deck at a distance of 2 m horizontally from the anti-collision wall. The measuring section corresponds to the position of the junction pier and suspender. The longitudinal arrangement is 8 m apart. Each measuring section is horizontally arranged with 2 measuring points; thus, there are 16 measuring sections of the whole bridge, a total of 32 measuring points. The comparison between the measured values and the theoretical values of the bridge deck alignment is shown in Figure 17, including both the left and right sides. It can be seen from Figure 17a that after the completion of the asphalt pavement bridge deck, the bridge deck alignment is smooth as a whole, which conforms to the change rule of theoretical calculation. Meanwhile, the smaller error of alignment results of deck elevation in Figure 17 can be used to justify the shape variation (either a parabola or hyperbola), as shown in Figure 14. According to the requirements of “Inspection and Evaluation Quality Standards for Highway Engineering” (JTG F80/1-2017), the allowable deviation of the deck elevation is calculated as Equation (2):

$$\text{Allowable deviation} = \pm(\text{Clear span}/5000 + 20), \quad (2)$$



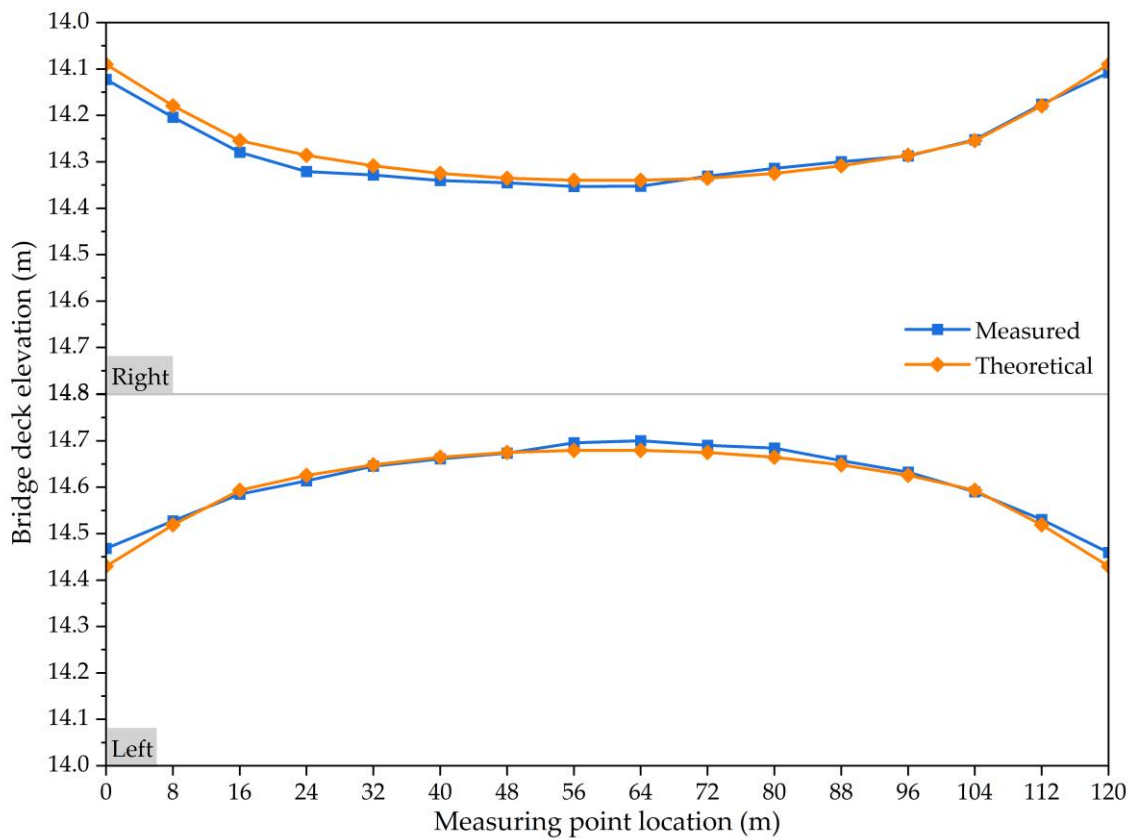
(a)



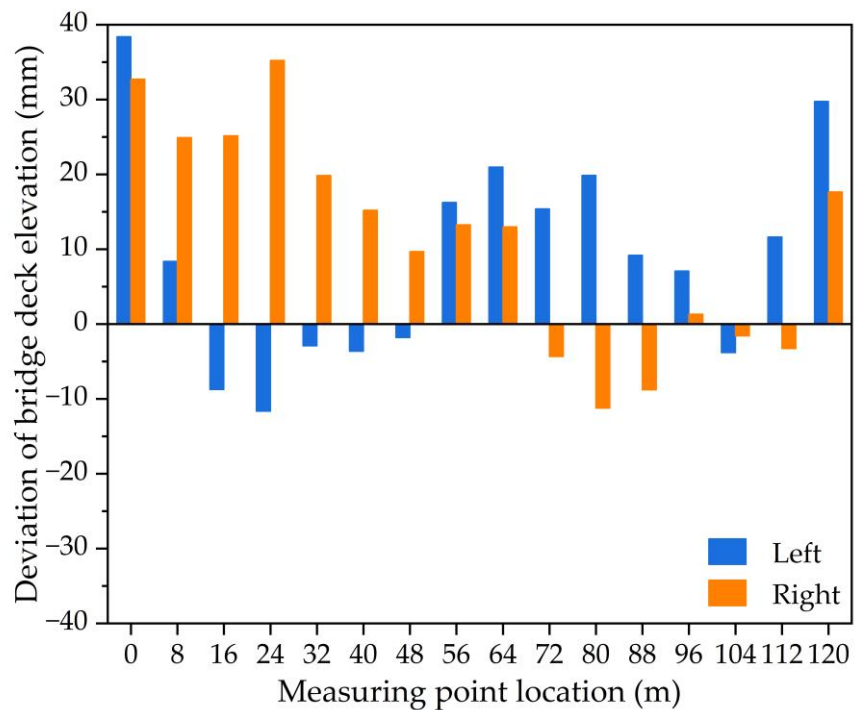
(b)

**Figure 16.** The cable force monitoring and calculated results of suspenders and tie rods after bridge construction completion: (a) comparison analysis of suspender cable force; (b) comparison analysis of tie rod cable force.

Through Equation (2), the allowable deviation of the deck elevation for the main bridge of the Dafeng River Bridge can be calculated as  $\pm(1,200,000/5000 + 20) = \pm 44$  mm. It can be seen from Figure 17b that after the completion of the bridge, the difference between the measured elevation and the theoretically expected elevation of the bridge deck is between  $-11.65$  mm and  $38.40$  mm, meeting the specification requirements. Overall, the deck elevation mainly exhibits downward deformation, with a small number of monitoring points showing upward deflection of the deck elevation, which may be caused by certain errors in actual monitoring values.



(a)



(b)

**Figure 17.** The alignment monitoring and calculated results of bridge deck elevation after bridge construction completion: (a) alignment comparison of deck elevation; (b) deviation of deck elevation.

## 7. Conclusions

This study carried out the symmetrical construction monitoring analysis and completed state evaluation of the newly built Dafeng River Bridge in Guangxi Province based on the finite element method. MIDAS Civil finite element software is used for simulation analysis to calculate the deformation and stress of the tied steel box arch bridge at the construction and completion stages and provide a theoretical basis for construction monitoring. Meanwhile, the alignment of the bridge deck and cable force of the suspender and tie rod of the bridge are measured. Based on the measured and theoretical calculation results, the completed state of the rigid frame-tied steel box arch bridge under symmetrical construction monitoring can be evaluated. From the simulation and monitoring results, the following conclusions can be drawn:

(1) The tensile and compressive stress of the main arch and transverse brace are symmetrically distributed, in which the maximum tensile stress is 15.1 MPa and the maximum compressive stress is 74.6 MPa, less than the specification allowable value of 245.5 MPa. The cumulative displacements of the main arch and lattice beam are symmetrically distributed and the largest at the midspan;

(2) Under the loading combinations of serviceability limit state and bearing capacity ultimate limit state, the stresses of the main arch, transverse brace, and lattice beam meet the specification requirements. The maximum cable forces of the suspender and tie rod under the bearing capacity ultimate limit state are 2189.4 kN and 2991.2 kN, and their corresponding minimum safety factors are (3.2 and 2.7), larger than the specified values (2.5 and 2.0);

(3) The camber of the main arch and lattice beam and the exact length of each suspender for the newly built Dafeng River Bridge can be determined through the finite element simulation calculation, taking into account various construction factors, which are used to guide the subsequent construction;

(4) Taking the cable force of the suspender and tie rod and the bridge deck alignment as the bridge construction quality evaluation index, based on the comparison analysis of the on-site monitoring and the finite element simulation calculation values, the deviations between the measured value and the theoretical value are within the specification allowable values, indicating that the bridge construction monitoring effect is reasonable and ideal.

**Author Contributions:** Conceptualization, J.P., X.W. and W.W.; methodology, J.P. and X.W.; validation, K.H.; formal analysis, J.P. and K.H.; investigation, X.W., K.H. and W.W.; writing—original draft preparation, J.P.; writing—review and editing, X.W., K.H. and W.W.; project administration, X.W. and W.W.; funding acquisition, X.W. and W.W. All authors have read and agreed to the published version of the manuscript.

**Funding:** This research was funded by the Science and Technology Base and Talent Special Project of Guangxi Province (grant number: AD21220121), the Scientific Research Project of the Department of Education of Jilin Province (grant number: JJKH20221019KJ), and the Postdoctoral Researcher Selection Funding Project of Jilin Province.

**Data Availability Statement:** Not applicable.

**Conflicts of Interest:** The authors declare no conflict of interest.

## References

1. Granata, M.F. Stressing Sequence for Hanger Replacement of Tied-Arch Bridges with Rigid Bars. *J. Bridg. Eng.* **2022**, *27*, 04021099. [[CrossRef](#)]
2. Yang, K.; Gao, L.; Zheng, K.; Shi, J. Mechanical behavior of a novel steel-concrete joint for long-span arch bridges—Application to Yachi River Bridge. *Eng. Struct.* **2022**, *265*, 114492. [[CrossRef](#)]
3. Deng, N.; Yu, M.; Yao, X. Intelligent Active Correction Technology and Application of Tower Displacement in Arch Bridge Cable Lifting Construction. *Appl. Sci.* **2021**, *11*, 9808. [[CrossRef](#)]
4. Huang, Q.; Wu, X.; Zhang, Y.; Ma, M. Proposed New Analytical Method of Tower Load in Large-Span Arch Bridge Cable Lifting Construction. *Appl. Sci.* **2022**, *12*, 9373. [[CrossRef](#)]

5. Tan, G.; Li, H.; Wang, W.; Kong, Q.; Jiang, L.; Zhang, S.; Wei, X. A rapid evaluation method based on natural frequency for post-earthquake traffic capacity of small and medium span bridges. *Eng. Struct.* **2023**, *280*, 115681. [[CrossRef](#)]
6. Tian, Z.; Zhang, Z.; Peng, W.; Dai, Y.; Cai, Y.; Xu, B. Research on the Method of Temporary Prestressing to Regulate the Stress in the Section during the Construction of the Main Arch Ring of the Cantilever Cast Arch Bridge. *Appl. Sci.* **2022**, *12*, 10070. [[CrossRef](#)]
7. Gao, H.; Zhang, K.; Wu, X.; Liu, H.; Zhang, L. Application of BRB to Seismic Mitigation of Steel Truss Arch Bridge Subjected to Near-Fault Ground Motions. *Buildings* **2022**, *12*, 2147. [[CrossRef](#)]
8. Mao, W.; Gou, H.; He, Y.; Pu, Q. Local Stress Behavior of Post-Tensioned Prestressed Anchorage Zones in Continuous Rigid Frame Arch Railway Bridge. *Appl. Sci.* **2018**, *8*, 1833. [[CrossRef](#)]
9. Huang, Q.; Wu, X.; Wei, H.; Chen, Q. Innovative Design of Novel Main and Secondary Arch Collaborative Y-Shaped Arch Bridge and Research on Shear Lag Effect of Its Unconventional Thin-Walled Steel Box Arch Ribs. *Appl. Sci.* **2022**, *12*, 8370. [[CrossRef](#)]
10. Zhang, Q.; Sun, T.; Wang, J.; Liu, Q. Deflection distribution estimation of the main arch of arch bridges based on long-gauge fiber optic sensing technology. *Adv. Struct. Eng.* **2019**, *22*, 3341–3351. [[CrossRef](#)]
11. Álvarez, J.; Aparicio, A.; Jara, J.; Jara, M. Seismic assessment of a long-span arch bridge considering the variation in axial forces induced by earthquakes. *Eng. Struct.* **2012**, *34*, 69–80. [[CrossRef](#)]
12. Morcous, G.; Hanna, K.; Deng, Y.; Tadros, M.K. Concrete-Filled Steel Tubular Tied Arch Bridge System: Application to Columbus Viaduct. *J. Bridg. Eng.* **2012**, *17*, 107–116. [[CrossRef](#)]
13. Xie, K.; Wang, H.; Guo, X.; Zhou, J. Study on the safety of the concrete pouring process for the main truss arch structure in a long-span concrete-filled steel tube arch bridge. *Mech. Adv. Mater. Struct.* **2021**, *28*, 731–740. [[CrossRef](#)]
14. Lederman, G.; You, Z.; Glišić, B. A novel deployable tied arch bridge. *Eng. Struct.* **2014**, *70*, 1–10. [[CrossRef](#)]
15. De Backer, H.; Outtier, A.; Van Bogaert, P. Buckling design of steel tied-arch bridges. *J. Constr. Steel Res.* **2014**, *103*, 159–167. [[CrossRef](#)]
16. Peng, Y.; Zhang, Z. Development of a Novel Type of Open-Web Continuous Reinforced-Concrete Rigid-Frame Bridge. *J. Bridg. Eng.* **2020**, *25*, 05020005. [[CrossRef](#)]
17. Huang, C.; Wang, Y.; Xu, S.; Shou, W.; Peng, C.; Lv, D. Vision-Based Methods for Relative Sag Measurement of Suspension Bridge Cables. *Buildings* **2022**, *12*, 667. [[CrossRef](#)]
18. Xu, Y.; Luo, Y.; Zhang, J. Laser-scan based pose monitoring for guiding erection of precast concrete bridge piers. *Autom. Constr.* **2022**, *140*, 104347. [[CrossRef](#)]
19. Puri, N.; Turkan, Y. Bridge construction progress monitoring using lidar and 4D design models. *Autom. Constr.* **2019**, *109*, 102961. [[CrossRef](#)]
20. Cheng, Y.; Lin, F.; Wang, W.; Zhang, J. Vision-based trajectory monitoring for assembly alignment of precast concrete bridge components. *Autom. Constr.* **2022**, *140*, 104350. [[CrossRef](#)]
21. Kim, D.; Kwak, Y.; Sohn, H. Accelerated cable-stayed bridge construction using terrestrial laser scanning. *Autom. Constr.* **2020**, *117*, 103269. [[CrossRef](#)]
22. Chen, Z.; Sun, H.; Zhou, S.; Chen, Z.; Xue, X.; Peng, Y. A hybrid algorithm for cable force calculation of cfst arch bridges during construction. *Int. J. Robot. Autom.* **2022**, *37*, 192–199. [[CrossRef](#)]
23. Gou, H.; Liu, C.; Bao, Y.; Han, B.; Pu, Q. Construction Monitoring of Self-Anchored Suspension Bridge with Inclined Tower. *J. Bridg. Eng.* **2021**, *26*, 05021011. [[CrossRef](#)]
24. Li, X.-X.; Ren, W.-X.; Bi, K.-M. FBG force-testing ring for bridge cable force monitoring and temperature compensation. *Sens. Actuators A Phys.* **2015**, *223*, 105–113. [[CrossRef](#)]
25. Ren, W.-X.; Lin, Y.-Q.; Peng, X.-L. Field Load Tests and Numerical Analysis of Qingzhou Cable-Stayed Bridge. *J. Bridg. Eng.* **2007**, *12*, 261–270. [[CrossRef](#)]
26. Gaute-Alonso, A.; Garcia-Sanchez, D.; Alonso-Cobo, C.; Calderon-Uriszar-Aldaca, I. Temporary cable force monitoring techniques during bridge construction-phase: The Tajo River Viaduct experience. *Sci. Rep.* **2022**, *12*, 7689. [[CrossRef](#)]
27. Bayraktar, A.; Akköse, M.; Taş, Y.; Erdiş, A.; Kurşun, A. Long-term strain behavior of in-service cable-stayed bridges under temperature variations. *J. Civ. Struct. Health Monit.* **2022**, *12*, 833–844. [[CrossRef](#)]
28. Jin, H.-W.; Wang, G.-A.; Chen, Z.-M. Temperature Control Technology for Construction of Jinsha River Bridge. *Adv. Civ. Eng.* **2021**, *2021*, 3452167. [[CrossRef](#)]
29. Mei, X.D.; Lu, Y.Y.; Shi, J. Temperature monitoring and analysis of a long-span cable-stayed bridge during construction period. *Struct. Monit. Maint.* **2021**, *8*, 203–220. [[CrossRef](#)]
30. Zhu, L.; Wang, Y.; Zhou, G.; Han, B. Structural health monitoring on a steel-concrete composite continuous bridge during construction and vehicle load tests. *Mech. Adv. Mater. Struct.* **2020**, *29*, 1370–1385. [[CrossRef](#)]
31. Grace, N.F.; Mohamed, M.E.; Kasabasic, M.; Chynoweth, M.; Ushijima, K.; Bebawy, M. Design, Construction, and Monitoring of US Longest Highway Bridge Span Prestressed with CFRP Strands. *J. Bridg. Eng.* **2022**, *27*, 04022047. [[CrossRef](#)]

**Disclaimer/Publisher's Note:** The statements, opinions and data contained in all publications are solely those of the individual author(s) and contributor(s) and not of MDPI and/or the editor(s). MDPI and/or the editor(s) disclaim responsibility for any injury to people or property resulting from any ideas, methods, instructions or products referred to in the content.